Measurements of directional properties of reverberant sound fields in rooms using a spherical microphone array

Gover, B. N.; Ryan, J. G.; Stinson, M. R.

Publisher's version / Version de l'éditeur:
https://doi.org/10.1121/1.1787525
Journal of the Acoustical Society of America, 116, October 4, pp. 2138-2148, 2004-10-01

Measurements of directional properties of reverberant sound fields in rooms using a spherical microphone array

Gover, B.N.; Ryan, J.G.; Stinson, M.R.

NRCC-46639

A version of this document is published in / Une version de ce document se trouve dans :
Journal of the Acoustical Society of America, v. 116 no. 4, Oct. 2004, pp. 2138-2148
Doi: 10.1121/1.1787525

Measurements of directional properties of reverberant sound fields in rooms using a spherical microphone array

Bradford N. Gover*†

Department of Physics, University of Waterloo, Waterloo, Ontario N2L 3G1, Canada, and Institute for Microstructural Sciences, National Research Council, Ottawa, Ontario K1A 0R6, Canada.

James G. Ryan‡ and Michael R. Stinson

Institute for Microstructural Sciences, National Research Council, Ottawa, Ontario K1A 0R6, Canada.

Received:

Suggested running title: Directional measurements of reverberant sound fields

Abbreviated title: Directional measurements of reverberant sound fields

*Electronic mail: brad.gover@nrc-cnrc.gc.ca

†Present Address: Institute for Research in Construction, National Research Council, Ottawa, Ontario K1A 0R6, Canada.

‡Present Address: Gennum Corporation, 232 Herzberg Rd., Kanata, Ontario K2K 2A1, Canada.

Abstract

The directional variation of sound at a point has been studied in three rooms, using a measurement system described previously [J. Acoust. Soc. Am. **112**, 1980–1991 (2002)]. The system uses a pair of 32-element spherical microphone arrays to obtain directional impulse responses in each of 60 steering directions, with an angular resolution of 28 degrees, covering all directions in the whole solid angle. Together, the array measurements span the frequency range from 300–3300 Hz. The angular distribution of incident sound energy is visualized on a three-dimensional plot, and quantified by computing the directional diffusion and the directional peak-to-average level difference ("anisotropy index") of the sound field. The small-to-medium sized rooms had reverberation times of 360, 400, and 600 ms. Measurements were made for several source and receiver locations in each, and were analyzed over several time ranges (full decay time of room, late time decay, 2 ms windows throughout the decay). All measured sound fields were found to be highly directional; the distribution of arriving energy at a point greatly influenced by the early specular reflections. The directions and arrival times of these reflections were identified from the measurements, giving excellent agreement with those expected from knowledge of the room geometry. It was observed that as time progressed, the sound fields initially exhibited increasing isotropy, followed by increasing *anisotropy*, due to nonuniform absorption in the rooms. The measurement system is capable of yielding detailed information about the reverberant sound field in a room, and is easily modified to be able to analyze ambient or time-varying fields.

PACS numbers: 43.55.Mc, 43.55.Gx, 43.55.Br, 43.38.Hz

I. INTRODUCTION

When studying the acoustics of reverberant spaces, the directional nature of the sound field is frequently of interest. Knowledge of how the sound field varies with direction at a point, and how this varies with time can potentially be of great value in areas such as auditorium assessment or correction,[1] determination of psychoacoustic indicators,[2] validation of diffuse field assumptions,[3] or in optimal microphone array design.[4] The direction and time of arrival of individual reflections, or an assessment of the overall diffuseness or isotropy of the field are commonly sought. The present study reports the results from the use of a new system to measure this information in sound fields in actual rooms.

Frequently, to study the sound field in a room, a single omnidirectional pressure microphone is used. Such measurements cannot yield spatial information as the directions of arrival of the component sound waves are lost. However, through inspection of a measured pressure-time signal, or more usually a room impulse response, the times of arrival of a few reflections are sometimes identifiable. Together with a detailed knowledge of the room geometry, it is occasionally possible to also identify reflecting surfaces and directions of arrival. This is not always possible, and even when it is, can be a significant amount of work.

The correlation of pressure measured at different points in a room can be used to infer confidence in the diffuseness of the field.[5,6] However, this technique is not without its shortcomings since the correlation coefficient deviates only weakly from its ideal diffuse values even in the presence of strong anisotropy.[7,8]

Measuring sound fields in rooms with an intensity probe, as is also common, can be useful in finding the directions of net energy transport.[9] Even measuring the intensity instantaneously does not necessarily aid in resolving reflections, however, since this direction of net energy flow is not always in the direction of a wavefront arrival. Analysis of intensity can, nevertheless, shed light on the overall diffuseness of the field.[10] There have been several studies reported in the past 10 years employing three-dimensional instantaneous intensity probes, including those by Oguro *et al.*,[11] Guy and Abdou,[12] Hori,[13] Peltonen *et al.*,[14] and

Merimaa *et al.*[15]

It is possible to employ multiple pressure microphones in a variety of ways to derive directionally-influenced information in a sound field. Examples of such studies include those by Yamasaki and Itow,[16] Sekiguchi *et al.*,[17] Täger and Mahieux,[18] Abel and Begault,[19] Essert,[20] and Becker *et al.*[21]

There is another group of existing studies that address the directional measurement problem by using a directional receiver or beamforming microphone array to look in one direction at a time. These include those by Thiele,[22] Broadhurst,[23] Nishi,[24] and Okubo *et al.*[25]

The present measurement system, described by the authors in Ref. 26, is also of this latter type, and is capable of detailed directional and temporal analysis. This system makes use of 32-microphone spherical arrays to achieve a highly directional beam pattern. Directional gains of over 14 dB are realized in 60 steering directions, with a 28 degree beamwidth. Responses can be analyzed instantaneously at each sample, or over arbitrary time windows. The measurements presented in this paper describe its application in three real rooms, and demonstrate how directional information is determined.

II. MEASUREMENT SYSTEM

The measurement system used in this work has been described in detail in Refs. 8 and 26. A block diagram summarizing the system is shown in Fig. 1. The system works as follows: A sound field is established in a room by playing a test signal over an omnidirectional loudspeaker. Simultaneously, a recording is made of the signals arriving at the microphones comprising the detecting array. The array has 32 elements, but in the present state of the system only 8 can be measured at a time, necessitating the repetition of the measurement 4 times. It is assumed that the system (room) being measured is time-invariant so that the identical sound field is established each of the 4 times. By using a maximum-length-sequence (MLS) to drive the loudspeaker, cross-correlation of the test signal with

each microphone signal results in the traditional (omnidirectional) room impulse responses at the array microphones.[27] Other stimuli may of course be used to measure the omnidirectional impulse responses.[28] Through subsequent beamforming in software, the array output is obtained in each of 60 steering directions. These outputs are the directional impulse responses—the pressure response at the array center due solely to sound arriving from within the directional array aperture.

At the heart of the system is the spherical microphone array. The geometrical arrangement of the 32 array microphones is that of a geodesic sphere, shown in Fig. 2. This arrangement lends itself naturally to the 60 symmetric steering directions, through the triangular faces of the polyhedron defined by the microphone positions (as vertices). Due to the symmetry, only one set of beamformer weights need be designed, which can be used to obtain the array output for all 60 steering directions from one set of measurements. The beamformer weights were designed from a constrained optimization procedure, maximizing the array gain subject to a constraint on the white noise gain.[26,29] The constraint was derived from measured magnitude and phase variances among the microphones, and serves to incorporate robustness to microphone noise and mismatch into the design. As a result, the array achieves a very high directionality over a broad range of frequency.

Over a range of about 1.7 octaves, the directional gain of the beam is above 14 dB, and the 3-dB beamwidth is 28 degrees. As a comparison, the familiar first-order hypercardioid pattern has a directional gain of 6 dB and a 3-dB beamwidth of 105°.[4] The position in frequency of the usable range of the array scales with the radius of the sphere (the breadth remains 1.7 octaves). To cover the range of frequencies from 300–3300 Hz, two arrays of different sizes were constructed. The construction of both employed 6 mm electret microphones (Panasonic WM-61A102B) mounted onto thin (1.6 mm) stainless steel rod frames. The arrays were both fitted with the same size support base to allow precise placement and repositioning. In replacing one array with the other to repeat a measurement over a different frequency range, the array centers were easily positioned at the same location. The larger of the arrays has a diameter of 48 cm and covers the range from 300–1000 Hz; the smaller has

a diameter of 16 cm and operates over 1000-3300 Hz. Plots of the beam pattern (averaged over the usable frequency range), and of the directional gain versus frequency for both arrays are shown in Fig. 3. These were calculated from the beamformer filters, using simulated anechoic data. The performance of the arrays was previously demonstrated in anechoic and reverberant chambers, and was found to be consistent with theoretical predictions.[26]

The control computer was equipped with a multichannel sound card (Echo Audio Layla24), which was used to play the MLS and simultaneously record from 8 of the array microphones. The omnidirectional loudspeaker (B&K Omnisource Type 4295) was driven by a power amplifier (Bryston 2B), and all playback/recording was controlled from software (Syntrillium Software CoolEdit SE). It is true that the loudspeaker becomes directional at higher frequencies, but up to 3300 Hz (the highest frequency of interest in this paper), it satisfies ISO standard requirements for omnidirectionality.[30] The microphone signals were sampled at a rate of 44.1 kHz but were downsampled prior to beamforming. The low-frequency array operates at a sampling rate of 2756.25 Hz, and the high-frequency array at a sampling rate of 11025 Hz.

III. SYSTEM OUTPUT AND ANALYSIS

As mentioned above, the time of arrival of discrete reflections is frequently identifiable from a room impulse response. With traditional omnidirectional responses, however, no information regarding from which direction the reflection arrives is available. In contrast, when inspecting a directional impulse response as measured with the present system, the direction of arrival of the reflection is clear. Fig. 4 illustrates these concepts for a measurement made in an anechoic chamber, in the presence of two parallel planar reflectors. On the omnidirectional response (panel (a)), the arrival time of the reflections is identifiable (7.5 ms), but it is not evident that two reflections arrive simultaneously. The directional measurements (panels (b)–(d)) clearly resolve the directions of arrival of both reflections, even though they arrive simultaneously.

The impulse response can be integrated to deduce the energy arriving at the receiving position over a given portion of the room decay. The energy E in a pressure impulse response $h(n)$ from time sample n_1 to time sample n_2 is proportional to the integral (sum) of the squared response:

$$E \propto \sum_{n=n_1}^{n_2} h^2(nT_s), \tag{1}$$

where $T_s = 1/F_s$ is the sampling period of a sequence sampled at rate F_s. This is the "incident" or "arriving" energy, assumed to be carried towards the receiving point by a plane wave. This quantity is proportional to the potential, and therefore total, energy of this plane wave. It is not the same as the total acoustic field energy at the receiving position. By computing the incident energy in each of a set of measured directional responses, the arriving energy versus direction can be graphed and/or analyzed. A normalized set of incident energies can be obtained from

$$e_i = \frac{\sum_{n=n_1}^{n_2} h_i^2(nT_s)}{\max_i \left\{ \sum_{n=n_1}^{n_2} h_i^2(nT_s) \right\}}, \tag{2}$$

where $h_i(n)$ is the directional impulse response for direction i.

Three-dimensional plots of e_i versus direction yield clear pictures of the direction of arrival of the incident sound energy (the directions between the 60 measured directions can be interpolated). This can be of use in identifying directions of significant or insignificant sound arrival. See Fig. 5, which depicts the incident energy distribution for the same parallel reflector measurement as discussed in Fig. 4. Panel (a) of the figure depicts the geometry of the measurement situation. Panel (b) shows the arriving energy versus all directions at once. Azimuth is indicated horizontally; elevation vertically along the curves. Panels (c) through (e) show three different views of the same surface, which plots the arriving energy as a function as direction. The radius and gray level of the surface in a particular direction indicate the energy incident from that direction. Notice that the direct sound and reflection pair are easily resolved.

The overall isotropy of the sound field can be assessed qualitatively from the plot, but also numerically from directional quantifiers. In particular, the directional diffusion and the peak-to-average level difference of the sound field can be easily computed.

The directional diffusion d is defined as[22,31]

$$d = \left(1 - \frac{\mu}{\mu_0}\right) \times 100\%, \tag{3}$$

with μ computed from

$$\mu = \frac{1}{\langle e \rangle} \sum_{i=1}^{60} |e_i - \langle e \rangle| \,, \tag{4}$$

where e_i is computed from the measured directional impulse responses via Eq. (2), and $\langle e \rangle$ is the mean incident energy over all directions, given by

$$\langle e \rangle = \frac{1}{60} \sum_{i=1}^{60} e_i. \tag{5}$$

The quantity μ is similar to the variance of the set of directional incident energies; μ_0 is the value for single plane-wave (anechoic) incidence and is determined by the beam pattern of the detector. d is merely a renormalization to change the range of values from 0% (anechoic) to 100% (isotropic). The system has been previously used to find a value of 21% in an anechoic chamber, and of 91% in a reverberation chamber.[26]

Since the incident energy in each directional response depends on the width of the receiver pattern, so too does d, and hence the same sound field measured with different receivers could yield differing values. With the present system, the same receiver is used in all cases, so comparisons among different measurements can be safely made.

The directional peak-to-average level difference L_{PA} of the sound field is obtained from

$$L_{PA} = 10 \log \left[\frac{\max(e_i)}{\langle e \rangle}\right], \tag{6}$$

the result being expressed in decibels. This is a quantity that is directly analogous to the directivity index (of a beam pattern), commonly used to describe the directionality of transducers and transducer arrays. It is logical therefore to refer to L_{PA} as the "anisotropy index" at the measurement point; it increases with increasing anisotropy of the sound field.

The anisotropy index takes on a minimum value of 0 dB when the sound field is perfectly isotropic. The microphone arrays used in the system have a beam pattern with a directivity index of about 14 dB, which is therefore the upper theoretical limit we can expect to measure. The system has been previously used to measure values of 12.8 dB and 1.5 dB in an anechoic and a reverberation chamber, respectively.[26]

It should be noted that by considering different values for n_1 and n_2 in Eq. (2) it is possible to plot the incident energy distribution and compute directional diffusion and anisotropy index at each time instant or for any given time range.

IV. FULL DECAY TIME

The length of the impulse responses measured with the system should be at least as long as the reverberation time of the room. This ensures detection of all arriving energy at the receiving point, from the direct arrival until the sound field has decayed by 60 dB. By integrating the squared impulse response over this entire time range, the energy in the full decay of the room is considered.

A. Small Meeting Room

Full decay time results for a measurement in a typical meeting room are shown in Fig. 6. The geometry of the room and source and array locations are shown in panel (a). The walls were wood-paneled, the floor had carpet over concrete, and the ceiling was acoustical tile. The room was fitted with a large table and 12 padded chairs (chairs not shown). The room dimensions were 4.14 m wide, 7.91 m long, and 3.13 m high. The broadband (300–3300 Hz) reverberation time was 360 ms. The distance from source to array was 3.14 m. Panel (b) shows the omnidirectional room impulse response measured with one of the array microphones. Panels (c)–(f) are the directional incident energy results measured with the high-frequency array (1000–3300 Hz): three views of the incident energy versus direction

surface, and the gray map depicting all directions at once. Panels (g)–(j) are corresponding plots for the low-frequency array measurement (300–1000 Hz).

As a qualitative observation, notice that the distribution was not isotropic. The directions of greater arriving energy are more or less the same as the indicated early-arriving (and strong) discrete reflections. Quantitatively, the value of the directional diffusion was 70% for the high-frequency measurement, and 73% for the low-frequency measurement. The value of the anisotropy index was 4.0 dB for the high-frequency measurement, and 4.2 dB for the low-frequency measurement.

1. Same source position, different receiver position

For the same source position in the same room, the array was moved to a new position and the measurement repeated. Care was taken to ensure that the source remained outside the near-field of the array, where the beamforming filters designed for plane-wave incidence would be inappropriate.[32] The full decay time results for the high-frequency measurement only are shown in Fig. 7, the layout being the same as panels (a)–(f) of Fig. 6. The low-frequency measurement is similar, and is omitted for brevity. Compared to the distribution in Fig. 6, the sound arriving at the array position for this case is clearly more anisotropic. The contribution from the direction of the source is larger, which is expected since the source-to-array distance was only 1.25 m for this measurement (as compared to 3.14 m previously). This observation is reinforced by the directional diffusion value of 59% and the anisotropy index value of 7.8 dB, as compared to 70% and 4.0 dB previously.

2. Same source-to-receiver separation

Full decay time results for a third measurement in the same meeting room are shown in Fig. 8, the layout being the same as Fig. 6, panels (a)–(f). In the interest of conciseness, only the high-frequency results are discussed. For this measurement, the source and array are in positions different than those used for the measurement presented in Fig. 6, but the

distance between them is the same. This means that the direct sound strength is the same in both cases, and therefore any differences in the isotropy are due to the room (reflections, scattering, etc.). Observe that there are differences in the "roundness" of the plot—evident in the comparison of panel (c) in particular. This observation is borne out by the value of anisotropy index (6.5 dB, compared to 4.0 dB previously), but interestingly not by the value of directional diffusion (71%, compared to 70% previously). The directional diffusion fails to indicate the difference between these sound fields.

B. Videoconferencing Room

Full decay time results for a measurement in a small videoconferencing room are shown in Fig. 9. The layout of the figure is the same as Fig. 6. The room was 7.23 m wide, 8.33 m long, 3.01 m high, had plaster walls, carpet over concrete floor, and acoustical tile ceiling. The room was fitted with a large table, several padded chairs (not shown), a cabinet housing videoconferencing equipment, and had a large heavy curtain covering the back wall. The broadband (300–3300 Hz) reverberation time was 400 ms. The source and array were positioned 2.03 m apart.

Notice again that the distribution of sound was not isotropic, and that the directions of the early-arriving discrete reflections shape the overall surface. A large proportion of the arriving energy is carried in these reflections. The value of the directional diffusion was 58% for the high-frequency measurement, and 57% for the low-frequency measurement. The value of the anisotropy index was 7.4 dB for the high-frequency measurement, and 8.6 dB for the low-frequency measurement.

C. Lecture Theater

Full decay time results for a measurement in a small lecture theater are shown in Fig. 10. The layout of the figure is the same as Fig. 6. The hall had plaster walls, a sloping, carpeted floor with 12 rows of upholstered, padded seats, and a sculpted ceiling. The room was

12.62 m wide and 16.45 m front-to-back. The height was 5.69 m at the front and 2.75 m at the back. The side walls were parallel. The broadband (300–3300 Hz) reverberation time was 600 ms, and the source and array were situated 4.01 m apart.

This room was larger than the other two, and the sound field was less diffuse, as evidenced by the directionality indicated in the figure. This is reinforced by the numerical values of directional diffusion and anisotropy index: respectively 61% and 5.5 dB for the high-frequency measurement, 62% and 6.8 dB for the low-frequency measurement.

V. TIME WINDOWING

Knowledge of the directional impulse responses is particularly useful for examining the isotropy of the sound field over restricted time ranges. For example, it can be of interest to gate out the discrete early arrivals, and examine only the reverberant tail. This was done for measurements in the three rooms. The high-frequency measurments only shall be discussed; the low-frequency measurements are similar.

A. Small Meeting Room

Fig. 11 shows several restricted time range results for a measurement with the high-frequency array in the small meeting room described in Sec. IV A. Panel (a) of the figure shows the room geometry and the source and array locations. Panel (b) shows the omnidirectional room impulse response measured at one of the array microphones. Panel (c) shows one view of the plot of full-decay-time arriving energy. Panel (d) shows a similar plot, but the energy arriving in the first 50 ms after the direct arrival is not included. This is the so-called "late" response only. Panel (e) is similar, but omits the first 100 ms of the response after the direct arrival.

Notice from panel (c) that in considering the full decay time of the room, there are significant sound contributions from the source direction (from the left) and from the reflections from above and below. The value of directional diffusion in this case is 64%, and that

of anisotropy index is 6.2 dB. The shape of the surface in panel (d) indicates that having gated the early arrivals out, the late sound is distributed more uniformly, but evidently is elongated along the long dimension of the room. The numerical indicators do indicate increased isotropy, having values of 77% for directional diffusion and 3.4 dB for anisotropy index. This elongated shape is even more pronounced in the plot of the later time range ($t > 100$ ms), seen in panel (e), which appears less-evenly distributed in direction. For this case, directional diffusion is 73% and anisotropy index is 4.4 dB, indeed indicating a more anisotropic distribution. There is longer-persisting sound propagating back-and-forth the length of the room, after having been absorbed in other directions.

B. Videoconferencing Room

Fig. 12 shows the restricted time range results for a measurement in the small videoconferencing room described in Sec. IV B, using the high-frequency array. The layout of the figure is the same as Fig. 11.

By comparing panels (c) and (d), notice that gating the early response results in a more uniform distribution of sound with direction, but not entirely so. The sound arriving in the late time period is in some ways more evenly distributed, but there is a strong back-and-forth component arriving laterally. These observations are reflected in the quantifiers directional diffusion and anisotropy index, which respectively were 67% and 6.7 dB for the full response, and 74% and 4.3 dB for the late response. It is interesting to note that for the later response ($t > 100$ ms), the quantifiers again indicate an increasing anisotropy (taking on values of 69% and 5.1 dB). As time progresses, sound is absorbed more quickly by the front and back walls than by the painted plaster side walls.

C. Lecture Theater

Fig. 13 shows the restricted time range results for a measurement in the small lecture theater described in Sec. IV C, using the high-frequency array. Panels (a)–(e) of the figure

are as in Figs. 11 and 12, plus an additional panel is added, (f), which shows results excluding the first 150 ms of arriving energy.

This extra time range was included to reveal the increasing anisotropy in this sound field as time passed. This behavior was not overly evident from inspecting the plots in panels (c)–(e), which do indicate increasing isotropy initially, as before. However, it can be seen that as the sound field decays, there are persistent arrivals back-and-forth across the room (between the parallel side walls). The directional diffusion and anisotropy index indicate this behavior as well, respectively having values of: 61% and 5.5 dB for the full decay time, 84% and 2.3 dB excluding the first 50 ms, 86% and 2.7 dB excluding the first 100 ms, and 81% and 3.8 dB excluding the first 150 ms. To observe this behavior in this larger room, more time is required to allow for sufficient reflections (i.e., sound absorptions) than in the smaller rooms.

VI. EVOLUTION OF THE SOUND FIELD

By considering the measured impulse responses over different ranges, it is possible to investigate the temporal evolution of the sound field, and to isolate discrete reflections in time and direction. For instance, computing the energy incident from each steering direction at each sample enables visualization of evolution of the sound field. Alternatively, by considering a short sliding time window, individual reflections can be located.

Fig. 14 shows results for a measurement made in the small lecture theater with the high-frequency array. Panel (a) shows the room geometry and the source and array locations. Panel (b) shows the omnidirectional room impulse response measured at one of the array microphones. Panel (c) shows the incident energy versus direction surface for the full decay time of the room. The plot has been superimposed on a three-dimensional drawing of the room. On a computer screen, this enables rotation and zooming to quickly identify room surfaces that cause reflections, for instance. Panel (d) shows likewise for the direct sound arrival, obtained by integrating the impulse responses from $t = 11$ ms to $t = 13$ ms only.

Panel (e) shows the reflection arriving at time $t = 30$ ms, which is the first-order reflection off the ceiling. The incident directions of the direct sound and this reflection were not known *a priori*—they followed from the measurements as output.

VII. CONCLUSIONS

The spherical array measurement system enables detailed analysis of reverberant sound fields. The measurements made in the three rooms discussed herein reveal not only the anisotropy of the sound fields, but details of that anisotropy in terms of time, direction, and overall quantification. The directions of the strong, early-arriving reflections are confirmed to be important, and are easily determined without the need for tedious measurement of the room geometry and inspection of omnidirectional impulse responses. It has been observed that source-to-array separation is important. However, for the same source-to-array separation, differences in diffusion related to position in the room were observed. It has further been noticed that the sound field in the larger room was less diffuse than those in the smaller rooms.

With this system, the time evolution and decay of the reverberant sound field can be investigated. Initially, the room reflections serve to "build up" the sound field at the receiving point in a manner which increases the isotropy. It was subsequently observed that the absorption of sound at different rates in different directions can lead to increasing anisotropy in the sound field as it decays.

All that is required to extend the present system to have the capability of analyzing non-reverberant (i.e., time varying) sound fields is the addition of 24 more simultaneous data acquisition channels. Such hardware is easily accessible nowadays, and such a modification would enable study of ambient sound fields, including human talkers or machinery noise, for example. It is hoped that the directional information measurable with the system can be of value in a range of application areas.

ACKNOWLEDGMENTS

The authors would like to thank to René St. Denis and John Quaroni at NRC for technical assistance. One author (BG) would additionally like to thank Dr. John Vanderkooy at the University of Waterloo for financial support and for many helpful discussions and suggestions.

REFERENCES

[1] L.L. Beranek, Music, Acoustics & Architecture (Wiley, New York, 1962).

[2] L. Cremer and H.A. Müller, Principles and Applications of Room Acoustics, Vol. 1, translated by T.J. Schultz (Applied Science Publishers, Essex, UK, 1982).

[3] A.D. Pierce, Acoustics: An Introduction to Its Physical Principles and Applications (Acoustical Society of America, New York, 1989).

[4] G.W. Elko, "Superdirectional Microphone Arrays," Chapter 10 of Acoustic Signal Processing for Telecommunication, edited by S.L. Gay and J. Benesty (Kluwer Academic, Norwell, MA, 2000).

[5] R.K. Cook, R.V. Waterhouse, R.D. Berendt, S. Edelman, and M.C. Thompson, "Measurement of correlation coefficients in reverberant sound fields," J. Acoust. Soc. Am. **27**, 1072–1077 (1955).

[6] C.T. Morrow, "Point-to-point correlation of sound pressures in reverberation chambers," J. Sound Vib. **16**, 29–42 (1971).

[7] T.J. Schultz, "Diffusion in reverberation rooms," J. Sound Vib. **16**, 17–28 (1971).

[8] B.N. Gover, "Development and use of a spherical microphone array for measurement of spatial properties of reverberant sound fields," Ph.D. thesis, Department of Physics, University of Waterloo, Waterloo, Canada, 2001.

[9] F.J. Fahy, Sound Intensity, 2nd ed. (E. & F.N. Spon, London, 1995).

[10] A. Abdou and R.W. Guy, "Spatial information of sound fields for room-acoustics evaluation and diagnosis," J. Acoust. Soc. Am. **100**, 3215–3226 (1996).

[11] S. Oguro, M. Anzai, H. Suzuki, and T. Ono, "A three-dimensional sound intensity probe," J. Acoust. Soc. Am. **91**, 2370(A) (1992).

[12] R.W. Guy and A. Abdou, "A measurement system and method to investigate the di-

rectional characteristics of sound fields in enclosures," Noise Control Eng. J. **42**, 8–18 (1994).

[13] K. Hori, "4 microphones power advanced, 3-dimensional sound intensity measuring system," Journal of Electronic Engineering, February, 47–49 (1994).

[14] T. Peltonen, T. Lokki, B. Gouatarbès, J. Merimaa, and M. Karjalainen, "A system for multi-channel and binaural room response measurements," Convention Paper 5289. Presented at the 110th Convention of the Audio Engineering Society, Amsterdam, The Netherlands, May 2001.

[15] J. Merimaa, T. Lokki, T. Peltonen, and M. Karjalainen, "Measurement, analysis, and visualization of directional room responses," Convention Paper 5449. Presented at the 111th Convention of the Audio Engineering Society, New York, USA, September 2001.

[16] Y. Yamasaki and T. Itow, "Measurement of spatial information in sound fields by closely located four point microphone method," J. Acoust. Soc. Jpn. (E) **10**, 101–110 (1989).

[17] K. Sekiguchi, S. Kimura, and T. Hanyuu, "Analysis of sound field on spatial information using a four-channel microphone system based on regular tetrahedron peak point method," Appl. Acoust. **37**, 305–323 (1992).

[18] W. Täger and Y. Mahieux, "Reverberant sound field analysis using a microphone array," Proceedings ICASSP-97, IEEE International Conference of Acoustics, Speech, and Signal Processing, Munich, Germany, April 1997.

[19] J.S. Abel and D.R. Begault, "Methods for room acoustic analysis using a monopole-dipole microphone array," Proceedings InterNoise98, Paper 123. International Congress on Noise Control Engineering, Christchurch, New Zealand, November 1998.

[20] R. Essert, "Progress in concert hall design—developing an awareness of spatial sound and learning how to control it," EBU Technical Review, Winter Issue, 31–39 (1997).

[21] J. Becker, M. Sapp, and O. Schmitz, "Four-microphone-array measurement combined with geometrical room acoustic technique," Collected papers from the 2nd Forum Acusticum/137th Meeting of the Acoustical Society of America, Oldenburg, Germany, 1999.

[22] R. Thiele, "Richtungsverteilung und Zeitfolge der Schallrückwurfe in Räumen," Acustica **3**, 291–302 (1953).

[23] A.D. Broadhurst, "An acoustic telescope for architectural acoustic measurements," Acustica **46**, 299–310 (1980).

[24] T. Nishi, "Relation between objective criteria and subjective factors in a sound field, determined by multivariate analyses," Acustica **76**, 153–162 (1992).

[25] H. Okubo, M. Otani, R. Ikezawa, S. Komiyama, and K. Nakabayashi, "A system for measuring the directional room acoustical parameters," Appl. Acoust. **62**, 203–215 (2001).

[26] B.N. Gover, J.G. Ryan, and M.R. Stinson, "Microphone array measurement system for analysis of directional and spatial variations of sound fields," J. Acoust. Soc. Am. **112**, 1980–1991 (2002).

[27] D.D. Rife and J. Vanderkooy, "Transfer-function measurement with maximum-length sequences," J. Audio Eng. Soc. **37**, 419–444 (1989).

[28] S. Müller and P. Massarani, "Transfer-function measurement with sweeps," J. Audio Eng. Soc. **49**, 443–471 (2001).

[29] H. Cox, R.M. Zeskind, and M.M. Owen, "Robust adaptive beamforming," IEEE Trans. Acoust., Speech, Signal Process. **35**, 1365–1376 (1987).

[30] Product Data Sheet for OmniSource Sound Source Type 4295, Brüel & Kjær, available from `www.bksv.com`.

[31] H. Kuttruff, Room Acoustics, 3rd ed. (Elsevier Applied Science, London, 1991).

[32] J.G. Ryan, "Criterion for the minimum source distance at which plane-wave beamforming

can be applied," J. Acoust. Soc. Am. **104**, 595–598 (1998).

List of Figures

1 Block diagram of measurement system. The microphone array steers a 28°-wide directional beam in 60 steering directions, detecting the sound arriving from each. 25

2 Array geometry depicting microphone locations (black dots) and the primary steering direction (+). The 32 microphone positions (those on back half of sphere not shown) lie at the vertices of a geodesic sphere (shown with dotted lines). The other steering directions are through the centers of the triangular faces of the polyhedron. 26

3 Array beam properties, computed from the beamformer coefficients: (a) Wide-band beam patterns for 16 cm array (dashed line) and 48 cm array (solid line), in the plane which passes through the primary steering direction, microphone 1, and the center of the array (see Fig. 2). The steering direction is at 0°, microphone 1 is at 21°. The asymmetry of the patterns are due to the asymmetry of the array with respect to this plane. (b) Directional gain versus frequency for 16 cm array (dashed line) and 48 cm array (solid line). . 27

4 Squared impulse responses measured for parallel reflectors in anechoic chamber (all self-normalized to have a maximum of unity): (a) Omnidirectional impulse response at one array microphone. Note the two symmetric reflections arriving at 7.5 ms are not resolvable in direction. (b) Directional impulse response in direction of source. The direct sound is picked up, but the pair of reflections is not. The peak at 6 ms is attributed to scattering from the loudspeaker support stand. (c) Directional impulse response in direction 61° to one side of the source direction. One lateral reflection is seen arriving at 7.5 ms. (d) Directional impulse response in direction 61° to the other side of the source direction. The other simultaneously-arriving lateral reflection is seen at 7.5 ms. 28

5 Results for parallel reflectors in anechoic chamber, measured with high-frequency array (1000–3300 Hz): (a) Geometry of the measurement setup. The line joining source and array is parallel to and equidistant from each reflecting panel. (b) Arriving sound energy as a gray scale map (azimuth horizontal, elevation vertical, measured from the array center). Directions of expected sound incidence (direct sound, a pair of first-order reflections) are indicated by white circles. (c)–(e) Three different views of the same measured data, plotted three-dimensionally versus azimuth and elevation. The radius and gray level of the surface are proportional to the arriving energy (in dB) in each direction. The directions of expected sound arrival are indicated by white arrows pointing inward. 29

6 Full decay time measurement in a small meeting room: (a) Geometry of room and source and array positions. (b) Omnidirectional room impulse response measured with one of the array microphones. (c)–(e) Three views of incident energy versus direction measured with the high-frequency array (1000–3300 Hz). (f) Arriving energy versus all directions measured with the high-frequency array. (g)–(i) Three views of incident energy versus direction measured with the low-frequency array (300–1000 Hz). (j) Arriving energy versus all directions measured with the low-frequency array. 30

7 Full decay time measurement with the high-frequency (1000–3300 Hz) array in a small meeting room, source in the same position as for the measurement shown in Fig. 6. Layout is the same as Fig. 6, panels (a)–(f). Note the increased anisotropy in this measurement as compared to that presented in Fig. 6. 31

8 Full decay time measurement with the high-frequency (1000–3300 Hz) array in a small meeting room, source-to-array distance the same as for the measurement shown in Fig. 6. Layout is the same as Fig. 6, panels (a)–(f). Note the increased anisotropy in this measurement as compared to that presented in Fig. 6. 32

9 Full decay time measurement in a videoconferencing room. Layout is the same as Fig. 6. 33

10 Full decay time measurement in a small lecture theater. Layout is the same as Fig. 6. 34

11 Restricted time range results for a measurement in the small meeting room, made with the high-frequency array (1000–3300 Hz). (a) Geometry of the room depicting source and array locations. (b) Omnidirectional impulse response measured at one of the array microphones. The vertical dotted lines indicate time cutoff points, 50 and 100 ms after the direct sound arrival. (c) One view of the arriving energy versus direction surface, including energy arriving over the full time of decay of the room. (d) Same as panel (c), but the energy arriving in the initial 50 ms is excluded. (e) Same as panel (c), but the energy arriving in the initial 100 ms is excluded. 35

12 Restricted time range results for a measurement in the videoconferencing room, made with the high-frequency array (1000–3300 Hz). Layout is the same as Fig. 11. 36

13 Restricted time range results for a measurement in the lecture theater made with the high-frequency array (1000–3300 Hz). Layout of panels (a)–(e) is the same as Fig. 11. Panel (f) shows the arriving energy versus direction, excluding the energy arriving in the first 150 ms after the direct sound arrival. 37

14 Time-windowed results for a measurement in the lecture theater made with the high-frequency array (1000–3300 Hz). (a) Geometry of the room, depicting the source (S) and array (A) positions. (b) Initial part of omnidirectional room impulse response measured with one of the array microphones. The vertical dotted lines indicate the short-time windows used to resolve the direct sound and one reflection. (c) Arriving energy versus direction plot superimposed on a drawing of the room, zoomed in on the array position. Energy integrated over full decay of room. (d) Same as panel (c), but incident energy integrated from $t = 11$ ms to $t = 13$ ms only. This shows the arrival of the direct sound. (e) Same as panel (c), but incident energy integrated from $t = 30$ ms to $t = 32$ ms only, revealing the arrival direction of a ceiling reflection. 38

FIGURES

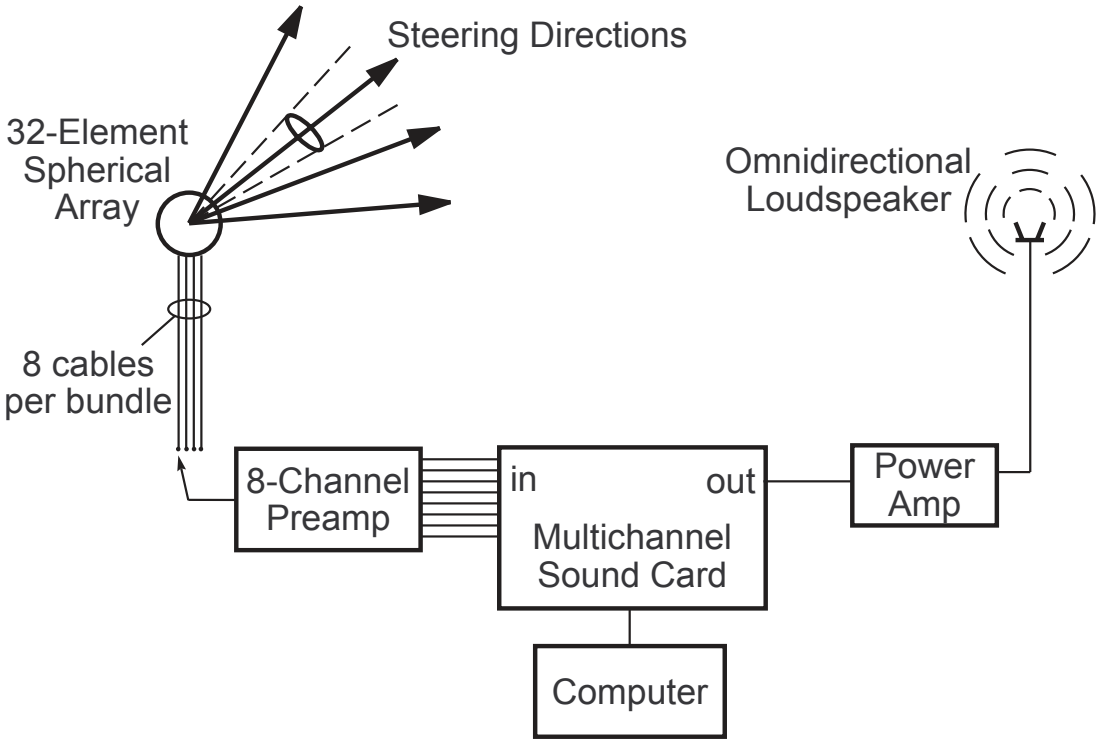

FIG. 1. Block diagram of measurement system. The microphone array steers a 28°-wide directional beam in 60 steering directions, detecting the sound arriving from each.

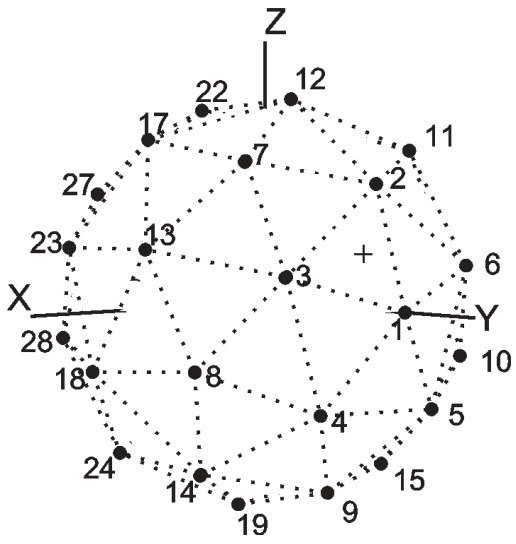

FIG. 2. Array geometry depicting microphone locations (black dots) and the primary steering direction (+). The 32 microphone positions (those on back half of sphere not shown) lie at the vertices of a geodesic sphere (shown with dotted lines). The other steering directions are through the centers of the triangular faces of the polyhedron.

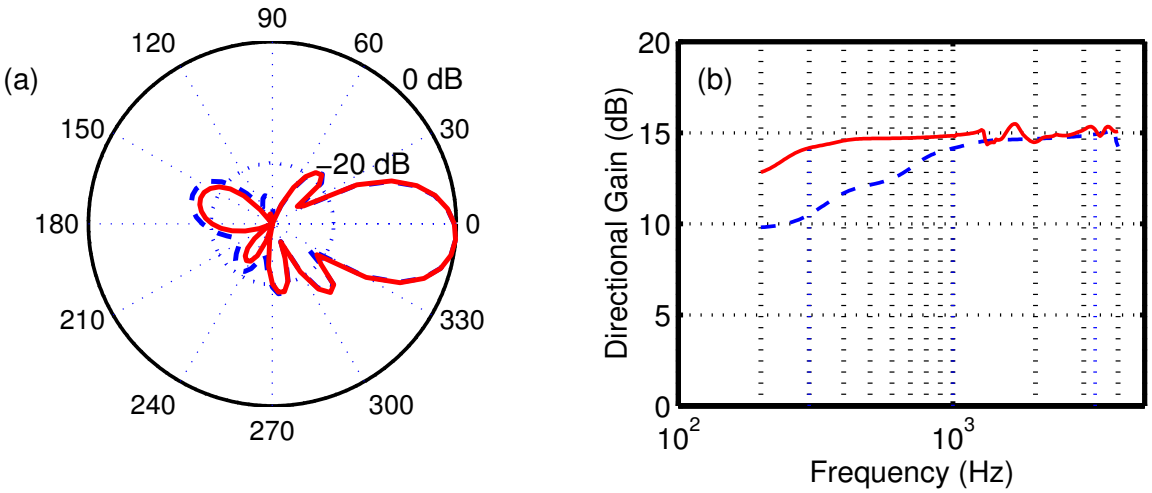

FIG. 3. Array beam properties, computed from the beamformer coefficients: (a) Wide-band beam patterns for 16 cm array (dashed line) and 48 cm array (solid line), in the plane which passes through the primary steering direction, microphone 1, and the center of the array (see Fig. 2). The steering direction is at 0°, microphone 1 is at 21°. The asymmetry of the patterns are due to the asymmetry of the array with respect to this plane. (b) Directional gain versus frequency for 16 cm array (dashed line) and 48 cm array (solid line).

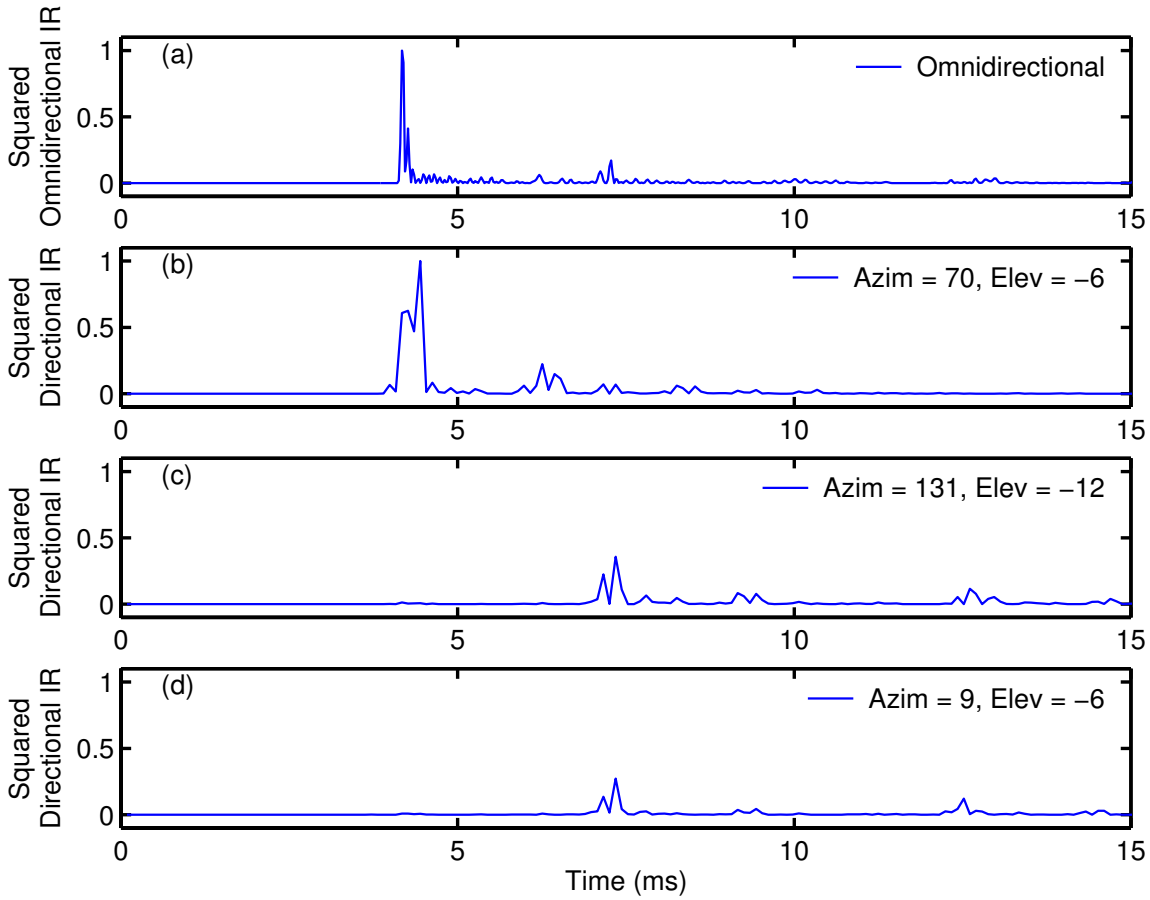

FIG. 4. Squared impulse responses measured for parallel reflectors in anechoic chamber (all self-normalized to have a maximum of unity): (a) Omnidirectional impulse response at one array microphone. Note the two symmetric reflections arriving at 7.5 ms are not resolvable in direction. (b) Directional impulse response in direction of source. The direct sound is picked up, but the pair of reflections is not. The peak at 6 ms is attributed to scattering from the loudspeaker support stand. (c) Directional impulse response in direction 61° to one side of the source direction. One lateral reflection is seen arriving at 7.5 ms. (d) Directional impulse response in direction 61° to the other side of the source direction. The other simultaneously-arriving lateral reflection is seen at 7.5 ms.

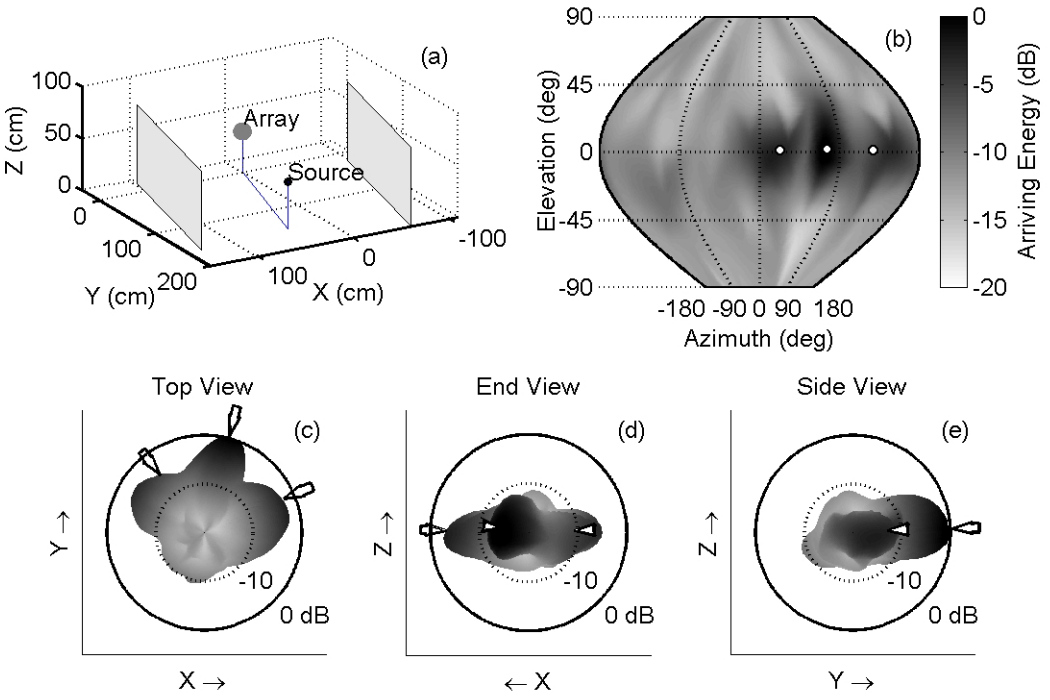

FIG. 5. Results for parallel reflectors in anechoic chamber, measured with high-frequency array (1000–3300 Hz): (a) Geometry of the measurement setup. The line joining source and array is parallel to and equidistant from each reflecting panel. (b) Arriving sound energy as a gray scale map (azimuth horizontal, elevation vertical, measured from the array center). Directions of expected sound incidence (direct sound, a pair of first-order reflections) are indicated by white circles. (c)–(e) Three different views of the same measured data, plotted three-dimensionally versus azimuth and elevation. The radius and gray level of the surface are proportional to the arriving energy (in dB) in each direction. The directions of expected sound arrival are indicated by white arrows pointing inward.

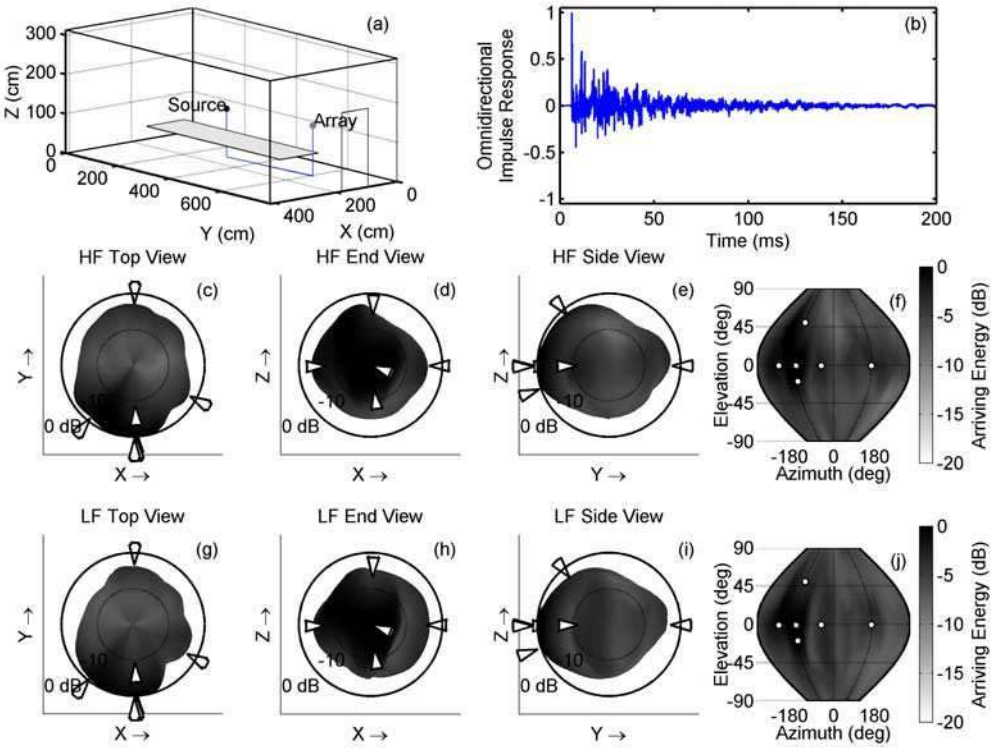

FIG. 6. Full decay time measurement in a small meeting room: (a) Geometry of room and source and array positions. (b) Omnidirectional room impulse response measured with one of the array microphones. (c)–(e) Three views of incident energy versus direction measured with the high-frequency array (1000–3300 Hz). (f) Arriving energy versus all directions measured with the high-frequency array. (g)–(i) Three views of incident energy versus direction measured with the low-frequency array (300–1000 Hz). (j) Arriving energy versus all directions measured with the low-frequency array.

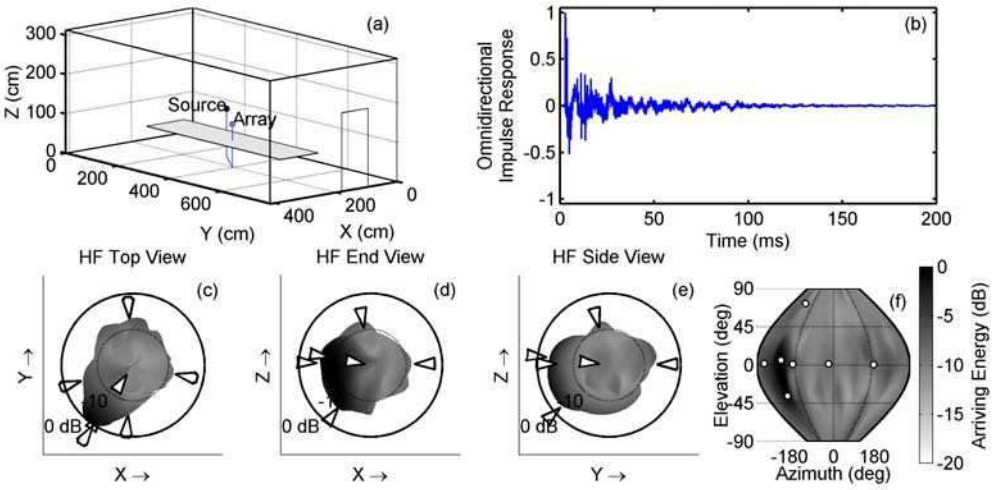

FIG. 7. Full decay time measurement with the high-frequency (1000–3300 Hz) array in a small meeting room, source in the same position as for the measurement shown in Fig. 6. Layout is the same as Fig. 6, panels (a)–(f). Note the increased anisotropy in this measurement as compared to that presented in Fig. 6.

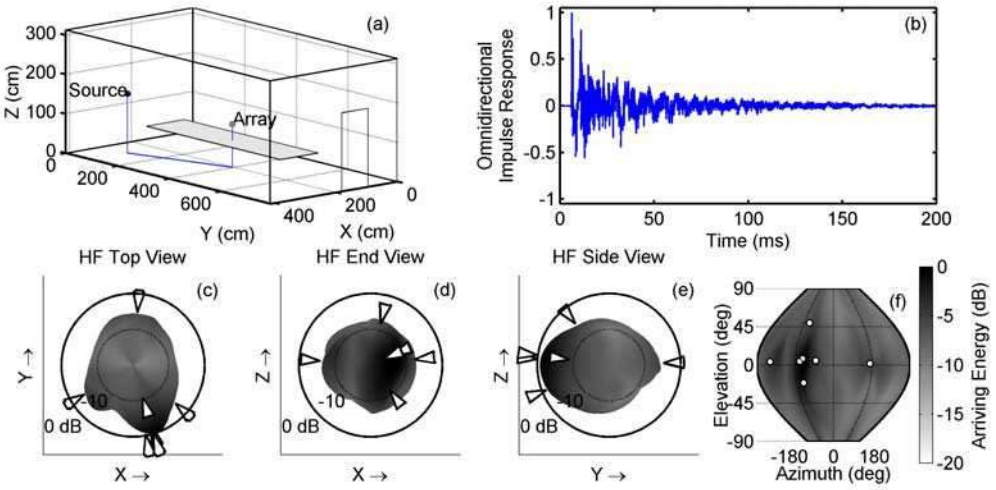

FIG. 8. Full decay time measurement with the high-frequency (1000–3300 Hz) array in a small meeting room, source-to-array distance the same as for the measurement shown in Fig. 6. Layout is the same as Fig. 6, panels (a)–(f). Note the increased anisotropy in this measurement as compared to that presented in Fig. 6.

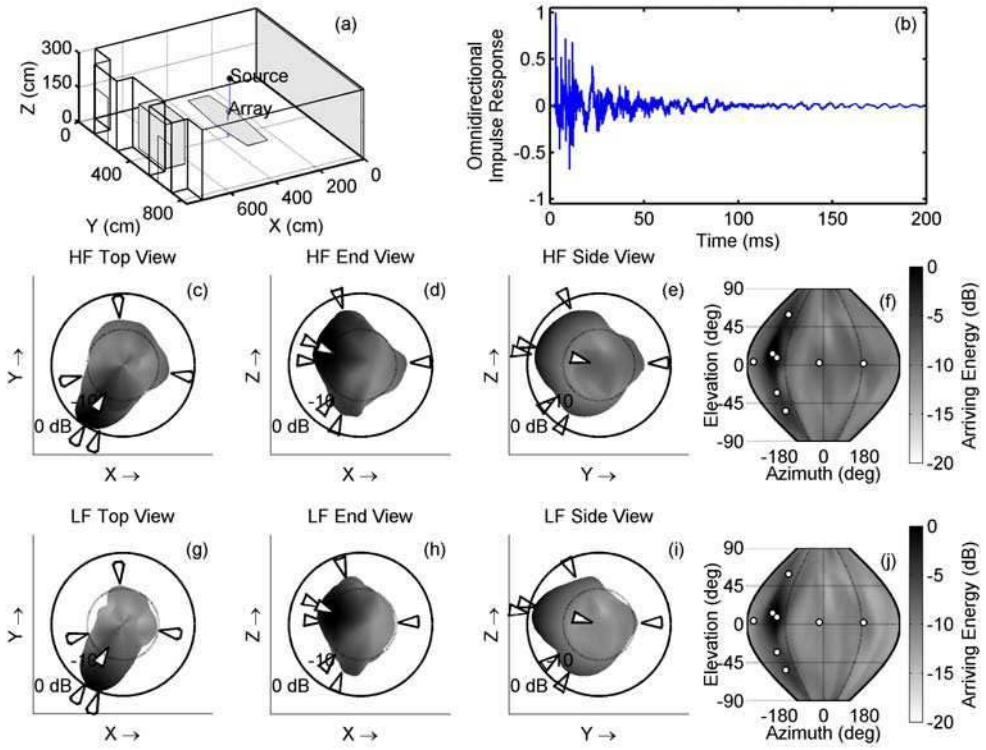

FIG. 9. Full decay time measurement in a videoconferencing room. Layout is the same as Fig. 6.

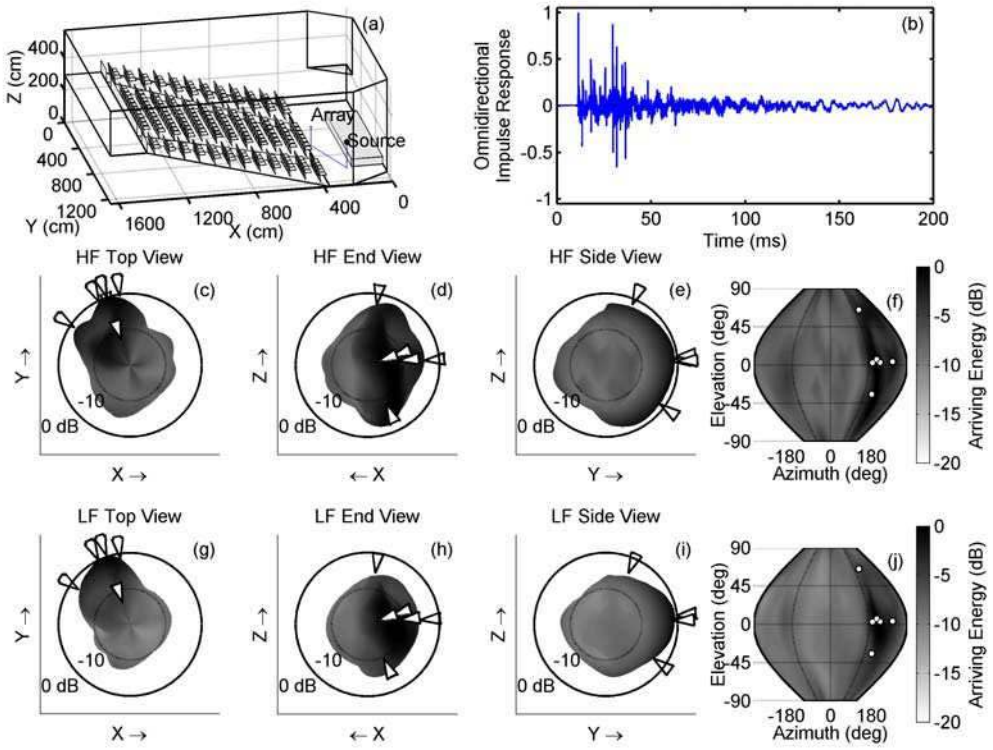

FIG. 10. Full decay time measurement in a small lecture theater. Layout is the same as Fig. 6.

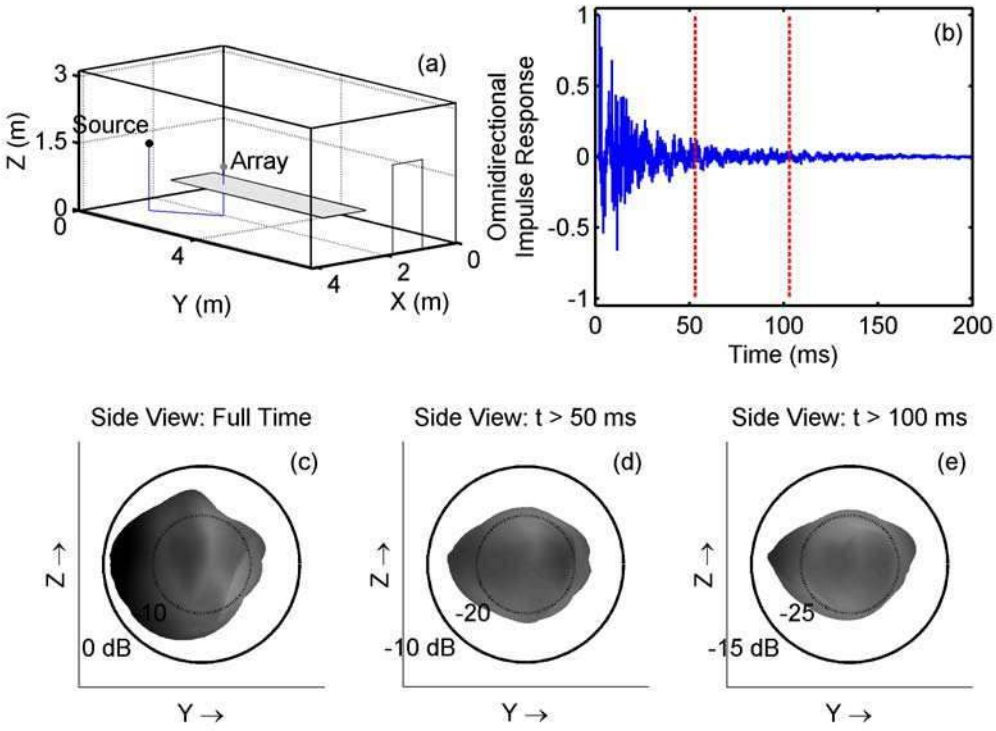

FIG. 11. Restricted time range results for a measurement in the small meeting room, made with the high-frequency array (1000–3300 Hz). (a) Geometry of the room depicting source and array locations. (b) Omnidirectional impulse response measured at one of the array microphones. The vertical dotted lines indicate time cutoff points, 50 and 100 ms after the direct sound arrival. (c) One view of the arriving energy versus direction surface, including energy arriving over the full time of decay of the room. (d) Same as panel (c), but the energy arriving in the initial 50 ms is excluded. (e) Same as panel (c), but the energy arriving in the initial 100 ms is excluded.

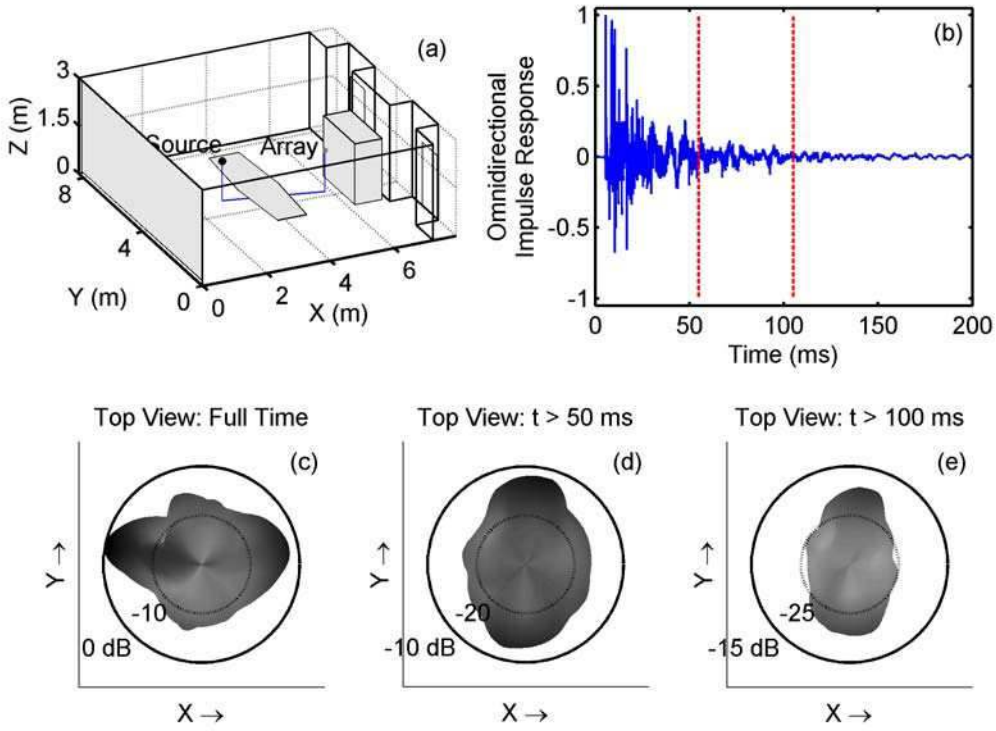

FIG. 12. Restricted time range results for a measurement in the videoconferencing room, made with the high-frequency array (1000–3300 Hz). Layout is the same as Fig. 11.

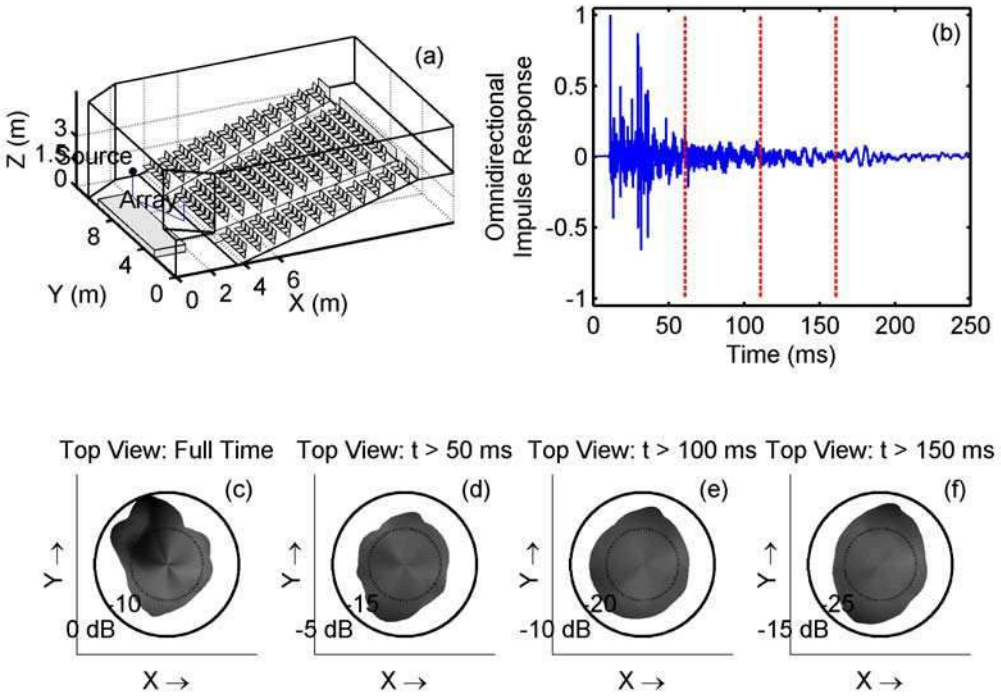

FIG. 13. Restricted time range results for a measurement in the lecture theater made with the high-frequency array (1000–3300 Hz). Layout of panels (a)–(e) is the same as Fig. 11. Panel (f) shows the arriving energy versus direction, excluding the energy arriving in the first 150 ms after the direct sound arrival.

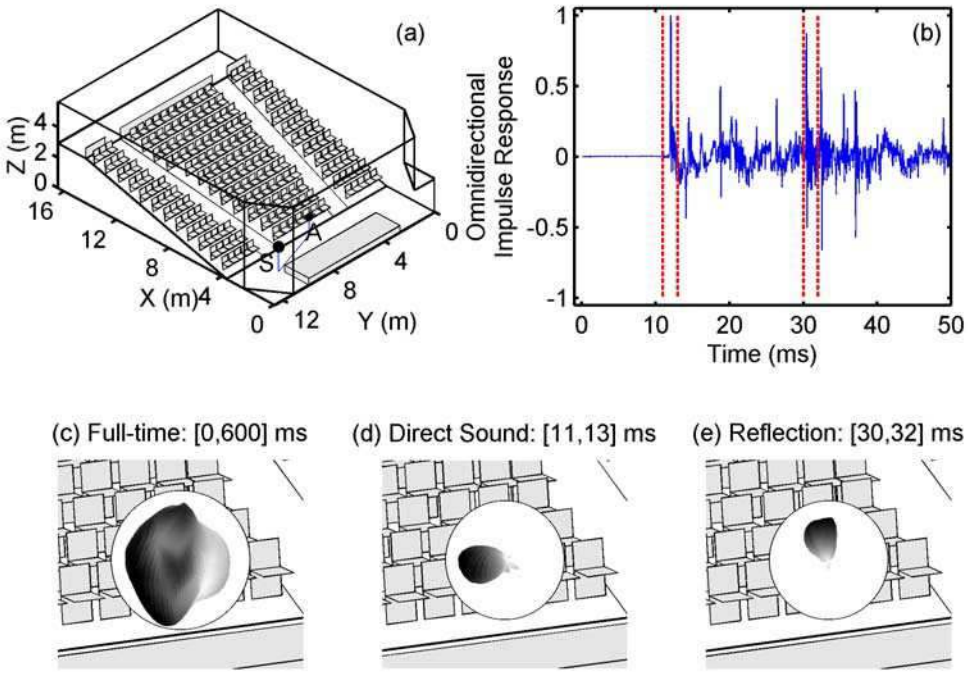

FIG. 14. Time-windowed results for a measurement in the lecture theater made with the high-frequency array (1000–3300 Hz). (a) Geometry of the room, depicting the source (S) and array (A) positions. (b) Initial part of omnidirectional room impulse response measured with one of the array microphones. The vertical dotted lines indicate the short-time windows used to resolve the direct sound and one reflection. (c) Arriving energy versus direction plot superimposed on a drawing of the room, zoomed in on the array position. Energy integrated over full decay of room. (d) Same as panel (c), but incident energy integrated from $t = 11$ ms to $t = 13$ ms only. This shows the arrival of the direct sound. (e) Same as panel (c), but incident energy integrated from $t = 30$ ms to $t = 32$ ms only, revealing the arrival direction of a ceiling reflection.